

# Electronic and magnetic properties of the $\text{RuX}_3$ ( $\text{X}=\text{Cl}, \text{Br}, \text{I}$ ) family: Two siblings — and a cousin?

David A. S. Kaib,<sup>1,\*</sup> Kira Riedl,<sup>2,†</sup> Aleksandar Razpopov,<sup>2</sup> Ying Li,<sup>3</sup> Steffen Backes,<sup>4</sup> Igor I. Mazin,<sup>5</sup> and Roser Valenti<sup>2,‡</sup>

<sup>1</sup>*Institut für Theoretische Physik, Goethe-Universität Frankfurt, 60438 Frankfurt am Main, Germany*

<sup>2</sup>*Institut für Theoretische Physik, Goethe-Universität, 60438 Frankfurt am Main, Germany*

<sup>3</sup>*Department of Applied Physics and MOE Key Laboratory for Nonequilibrium Synthesis and Modulation of Condensed Matter, School of Physics, Xi'an Jiaotong University, Xi'an 710049, China*

<sup>4</sup>*CPHT, CNRS, Ecole Polytechnique, Institut Polytechnique de Paris, Route de Saclay, 91128 Palaiseau, France*

<sup>5</sup>*Department of Physics and Astronomy and Quantum Science and Engineering Center, George Mason University, Fairfax, Virginia 22030, United States*

(Dated: August 17, 2022)

Motivated by reports of metallic behavior in the recently synthesized  $\text{RuI}_3$ , in contrast to the Mott-insulating nature of the actively discussed  $\alpha\text{-RuCl}_3$ , as well as  $\text{RuBr}_3$ , we present a detailed comparative analysis of the electronic and magnetic properties of this family of trihalides. Using a combination of first-principles calculations and effective-model considerations, we conclude that  $\text{RuI}_3$ , similarly to the other two members, is most probably on the verge of a Mott insulator, but with much smaller magnetic moments and a strong magnetic frustration. We predict the ideal pristine crystal of  $\text{RuI}_3$  to have a nearly vanishing conventional nearest-neighbor Heisenberg interaction and to be a quantum spin liquid candidate of possibly different kind than the Kitaev spin liquid. In order to understand the apparent contradiction to the reported resistivity  $\rho$ , we analyze the experimental evidence for all three compounds and propose a scenario for the observed metallicity in existing samples of  $\text{RuI}_3$ . Furthermore, for the Mott insulator  $\text{RuBr}_3$  we obtain a magnetic Hamiltonian of a similar form to that in the much discussed  $\alpha\text{-RuCl}_3$  and show that this Hamiltonian is in agreement with experimental evidence in  $\text{RuBr}_3$ .

## INTRODUCTION

$\text{RuI}_3$  and  $\text{RuBr}_3$  are recent additions to the  $\text{RuX}_3$  family ( $\text{X}=\text{Cl}, \text{Br}, \text{I}$ ) of layered Ru-based trihalides (Fig. 1a). The first member,  $\alpha\text{-RuCl}_3$  (in the following ‘ $\text{RuCl}_3$ ’) has attracted considerable attention in recent years as a candidate material for the Kitaev honeycomb model [1].  $\text{RuCl}_3$  is a spin-orbit assisted Mott insulator [2–5] whose magnetic low-energy degrees of freedom can be described in terms of  $j_{\text{eff}} = 1/2$  moments that interact through strongly anisotropic exchange [2, 6–8]. While the material enters a so-called zigzag antiferromagnetic order (Fig. 1b) at low temperatures  $T_N \approx 7\text{ K}$  [4, 9, 10], various experiments at finite temperature [11–14] or at finite magnetic field [4, 15–18] have been interpreted as hallmarks of Kitaev physics, a subject which is presently under intensive debate [19–24]. Recently, a sister compound with a heavier halogen,  $\text{X} = \text{Br}$ , was synthesized [25]. Analogous to  $\text{RuCl}_3$ , it is insulating and shows zigzag magnetic order, albeit with higher Néel temperature  $T_N = 34\text{ K}$  [25]. In contrast to  $\text{RuCl}_3$ , the authors of Ref. 25 reported a Weiss constant with dominant antiferromagnetic interactions and a direction of the zigzag ordered moment different from  $\text{RuCl}_3$ , and argued that this deviation suggests a closer proximity to the pure Kitaev model.

To complete the  $\text{RuX}_3$  family, two independent groups have now synthesized  $\text{RuI}_3$  with the even heavier halogen iodine [26, 27]. In contrast to the two ‘sibling’ compounds, a quasi-metallic behavior was observed in  $\text{RuI}_3$ , questioning

the description in terms of localized  $j_{\text{eff}} = 1/2$  moments. Even though the dc resistivities measured in  $\text{RuI}_3$  are orders of magnitude smaller than those of  $\text{RuCl}_3$  or  $\text{RuBr}_3$ , the reported values of  $10^{-3}$  to  $10^{-2}\ \Omega\text{ cm}$  [26] are uncharacteristically large for metals or even typical bad metals [28], and practically temperature-independent. While neither of the groups found clear signatures of magnetic ordering [26, 27], they reported different behaviors of the magnetic susceptibility, which is either found to be temperature-independent [26], or with a strong upturn at low temperatures [27], suggesting that sample quality plays a crucial role.

In order to understand the apparently distinct behavior of this family of trihalide materials, in this work we analyze the available experimental data and perform a detailed comparative study of the electronic and magnetic properties of the systems via first-principles calculations and extracted low-energy models. We find that: (i) The behavior of  $\text{RuI}_3$  is not that far from  $\text{RuCl}_3$  and  $\text{RuBr}_3$  and the variations across the series are more quantitative than qualitative. (ii) Pristine samples of  $\text{RuI}_3$  should be insulating with highly anisotropic magnetic exchange and nearly vanishing conventional Heisenberg interaction. We argue that the reported metallic behavior in  $\text{RuI}_3$  could have its origin in sample quality. (iii) The magnetism in the Mott insulator  $\text{RuBr}_3$  has predominantly ferromagnetic interactions, in contrast to what is suggested by the Curie-Weiss analysis of Ref. [25]. We show that such interactions are consistent with experiment when taking into account spin-orbit coupling effects in the Curie-Weiss behavior.

Our study derives model parameters and magnetic Hamiltonians for the whole  $\text{RuX}_3$  family from *ab-initio*, that will be useful for future theoretical studies of these systems. In contrast to the usual model derivations that only include lo-

\* kaib@itp.uni-frankfurt.de

† riedl@itp.uni-frankfurt.de

‡ valenti@itp.uni-frankfurt.de

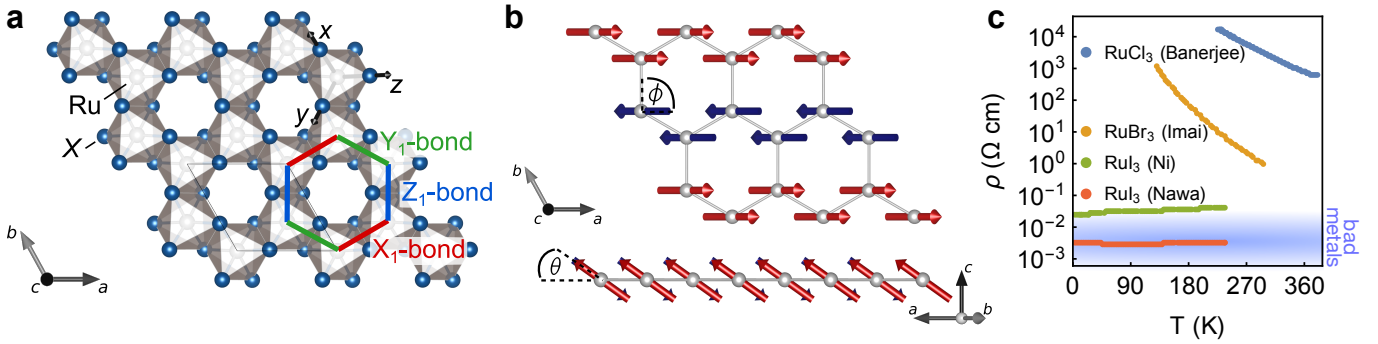


FIG. 1.  $\text{RuX}_3$  ( $X=\text{Cl, Br, I}$ ) crystal structure, magnetic structure and resistivity. **a** Honeycomb layer in the  $\text{RuX}_3$  ( $X=\text{Cl, Br, I}$ ) trihalides with bond definitions, cubic axes ( $xyz$ ) and crystallographic axes ( $abc$ ) in the  $R\bar{3}$  structure, **b** Zigzag magnetic order in a honeycomb layer from two perspectives, with definitions of in-plane-angle  $\phi$  and out-of-plane-angle  $\theta$ . **c** Comparison of experimental dc resistivities as a function of temperature. Data was extracted from plots in the following references and labelled by respective first-author names:  $\text{RuCl}_3$  (Banerjee [10]),  $\text{RuBr}_3$  (Imai [25]),  $\text{RuI}_3$  (Ni [27], Nawa [26]). The shaded background depicts a typical range of resistivity for bad metals [28].

cal spin-orbit coupling (SOC) on the magnetic ion [2, 6, 8], our approach includes all SOC effects in the crystal. In fact, we show that SOC from the ligands leads to significant deviations from the Ruthenium-only SOC picture in the case of  $\text{RuBr}_3$  and  $\text{RuI}_3$ .

## RESULTS AND DISCUSSION

### Comparative analysis of experiments

In the following, we analyze the reported electrical resistivity, specific heat and magnetic susceptibility data for  $\text{RuX}_3$  ( $X=\text{Cl, Br, I}$ ) [10, 25–27, 29].

In Fig. 1c we summarize the temperature dependence of the experimental resistivity data [10, 25–27] in all three compounds. In  $\text{RuI}_3$ , the resistivity has a weak [27] or almost no [26] temperature dependence (Fig. 1c). Traditionally, metals are classified as materials where the resistivity  $\rho$  increases with temperature, distinguishing conventional metals (*e.g.*, Cu) as those where in clean samples at temperatures roughly 300 to 600 K,  $\rho \sim 10^{-6} \Omega \cdot \text{cm}$  to  $\sim 10^{-5} \Omega \cdot \text{cm}$ , and bad metals as those with resistivities of  $\sim 1 - 10 \text{ m}\Omega \cdot \text{cm}$ . This range is shown as a background shading in Fig. 1c. The reported resistivities for  $\text{RuI}_3$  ( $\rho \sim 40 \text{ m}\Omega \cdot \text{cm}$  [27] and  $\rho \sim 4 \text{ m}\Omega \cdot \text{cm}$  [26]) are high even for bad metals, surpassing the Ioffe-Regel limit by more than an order of magnitude. Even more relevant, the lower-resistivity set of data [26] shows no discernible temperature dependence at all, while the data in Ref. 27 show a very weak positive derivative  $d\rho/dT$ , but the absolute value is above anything traditionally considered metallic.

Seemingly, as also pointed out in Ref. 27, electron transport in existing  $\text{RuI}_3$  samples may be contaminated by grain boundaries. One possibility to interpret the measurements is that the pristine material is metallic, but insulating grain boundaries prevent percolation. Then, the in-grain resistivity can be neglected and what is measured is the resistivity of the insulating grain boundaries. In that case, however, thermal activation of carriers in the boundaries

should give a positive temperature gradient of the resistivity, which is not observed. The opposite scenario is that of an insulating behavior in the bulk and (possibly bad) metallic one between the grains. In that case, the large resistivity reflects the small relative volume of metallic boundaries, where the transport is dominated by the residual resistivity. This scenario is compatible with the observations. Morphology of the grain boundaries can vary wildly depending on the growth conditions, including but not limited to vacancies, twins, dislocation and plain chemical dirt. Grain boundaries in semiconductors are often observed to be metallic. Apart from grain boundaries contaminating resistivity measurements, disorder (in form of vacancies, stacking faults, etc. [26, 27]) could promote the bulk metallic phase over the Mott-insulating one, as has been shown for example for the Mott insulator  $\kappa\text{-(BEDT-TTF)}_2\text{Cu}[\text{N}(\text{CN})_2]\text{Cl}$  [30]. Indeed, in our first-principles calculations discussed below, we find the ideal  $\text{RuI}_3$  to already be quite close to a Mott-metal transition.

Turning to the sibling compounds  $\text{RuCl}_3$  and  $\text{RuBr}_3$ , the resistivity (Fig. 1c) decreases with temperature, as expected for Mott insulators, and both systems show an approximate exponential activation gap behavior,  $E_{g,\text{eff}}(T) = -k_B T^2 (d \ln \rho / dT)$ , although with a significant blue-shift of the gap with increasing temperatures.

Considering specific heat data in the compounds, the specific heat for  $\text{RuCl}_3$  displays a well-defined peak at  $T_N \approx 7 \text{ K}$  denoting the onset of the zigzag order, while the onset of long-range magnetic order in  $\text{RuBr}_3$  is observed by a kink at  $T_N = 34 \text{ K}$  [25]. None of this is observed for  $\text{RuI}_3$  [26, 27]. In Table 1 we summarize specific heat parameters reported experimentally [25–27, 31], where  $\gamma$  ( $\beta$ ) is the  $T$ -linear ( $T^3$ ) contribution to  $C(T)$ .

In  $\text{RuI}_3$ , the  $T$ -linear contribution, even though contaminated by an extrinsic raise at small temperatures in Ref. [27] attributed to the nuclear quadrupole moment of Ru, yields  $\gamma \sim 15 - 30 \text{ mJ} \cdot \text{K}^{-2} \cdot \text{mol}^{-1}$  [26, 27]. From our electronic structure calculations of  $\text{RuI}_3$  shown below, we

Sample	$\gamma$	$\beta$	$T_D$	$T_D M_{\text{RuX}_3}^{1/2}$
RuCl <sub>3</sub> * (Tanaka [31])		1.22	185	1
RuBr <sub>3</sub> (Imai [25])		1.93	159	1.21
RuI <sub>3</sub> (Ni [27])	29.3	4.72	118	1.07
RuI <sub>3</sub> (Nawa [26])	17.7	3.66	129	1.17

TABLE 1. **Overview of reported specific heat parameters.**  $\gamma$  ( $\beta$ ) is the coefficient of the  $T$ -linear ( $T^3$ ) contribution and given in units of  $\text{mJ}\cdot\text{K}^{-2}\cdot\text{mol}^{-1}$  ( $\text{mJ}\cdot\text{K}^{-4}\cdot\text{mol}^{-1}$ ). Debye temperature  $T_D = \left(\frac{12\pi^4 N R}{5\beta}\right)^{1/3}$  is given in Kelvin and  $T_D M_{\text{RuX}_3}^{1/2}$  as a ratio to the value for RuCl<sub>3</sub> (first row), where  $M_{\text{RuX}_3}$  is the harmonic average of the  $\text{RuX}_3$  mass. (\*) Note that the values given for RuCl<sub>3</sub> correspond to the asymptotic field-polarized limit extracted by Tanaka *et al.* [31], as otherwise at zero field the low-temperature specific heat behavior is dominated by vicinity to the Néel temperature of RuCl<sub>3</sub>, causing large magnetic contributions to  $\beta$ .

find that the unrenormalized metallic (*i.e.*, nonmagnetic, not  $U$ -corrected) density of states corresponds to  $\gamma_0 \approx 3 \text{ mJ}\cdot\text{K}^{-3}\cdot\text{mol}^{-1}$ , suggesting a mass renormalization (if this  $\gamma$  is intrinsic) of a factor of 7–12. In the scenario where the metallic grain boundaries take up a sizeable fraction of the sample volume, this renormalization shall be even stronger, encroaching into the heavy fermions domain. This suggests that the origin of the anomalously large residual heat capacity may not be related to intrinsic metallicity. It is worth noting that the  $T^3$  term  $\beta$  of  $C(T)$ , on the other hand, is rather reasonable for the three systems and scales roughly as the harmonic average  $M_{\text{RuX}_3}$  of the atomic masses (last column in Table 1).

We now turn our attention to magnetic susceptibility measurements. Figure 2a summarizes the powder-averaged measured magnetic susceptibilities  $\chi(T)$  as reported in Refs. [25–27, 32]. At low temperatures the RuCl<sub>3</sub> data [32] shows a clear signature of a transition to the ordered magnetic phase at 7 K. For RuBr<sub>3</sub>, the Néel transition  $T_N \approx 34$  K is less apparent from the susceptibility, but the maximum in  $d\chi/dT$  is consistent with the distinct transition seen in NMR relaxation measurements [25]. The experimental report on powder samples of RuBr<sub>3</sub> utilized a standard Curie-Weiss (CW) fit, yielding an average Curie-Weiss temperature  $\Theta_{\text{std}}^{\text{avg}} = -58$  K [25], indicating predominantly AFM interactions. However, as we have recently shown [33], the Weiss constants obtained with such a standard CW fit may not anymore reflect the intrinsic exchange couplings in the case of significant SOC in the material, as it is the case for the Ru-based trihalides. With SOC, temperature-dependent van-Vleck contributions can arise, which can be effectively captured in a temperature-dependent magnetic moment  $\mu_{\text{eff}}(T, \Delta)$  [33], as shown for  $\Delta = 0.018$  eV in Fig. 2b, where  $\Delta$  can be directly associated to the crystal field splitting resulting from the distorted octahedral environment of Ru. In fact, for the sister compound RuCl<sub>3</sub>, a standard CW fit would lead to  $\Theta_{\text{std}}^{\text{avg}} = -20$  K, whereas an improved CW fit taking into account such *van-Vleck*-like contributions [33] provides CW constants  $\Theta^{\parallel} = +55$  K for the magnetic field in the honeycomb plane and  $\Theta^{\perp} = +33$  K

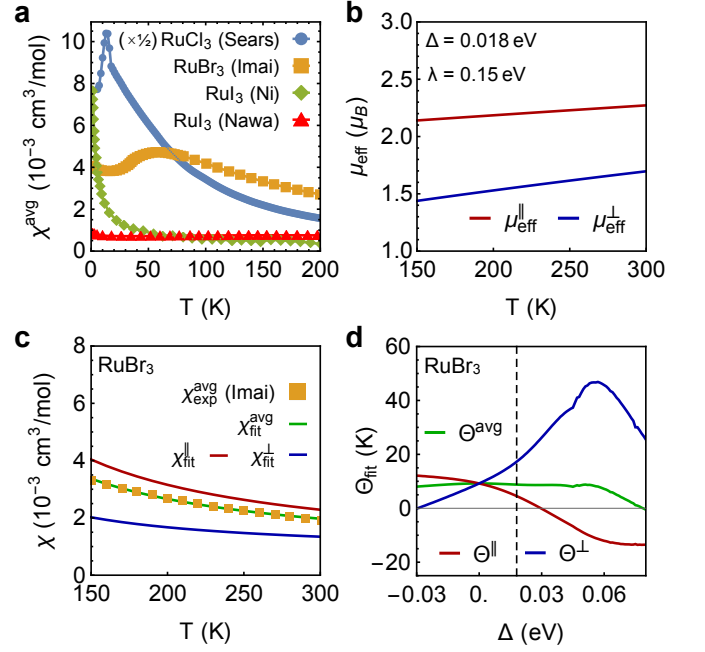


FIG. 2. **Magnetic susceptibility and modified Curie-Weiss fit.** **a** Experimental direction-averaged  $\text{RuX}_3$  susceptibility data, extracted from plots in the following references and labelled by respective first-author names: RuCl<sub>3</sub> (Sears) [32], RuBr<sub>3</sub> (Imai) [25], RuI<sub>3</sub> (Ni) [27], RuI<sub>3</sub> (Nawa) [26]. Note that the RuCl<sub>3</sub> curve is scaled by  $\frac{1}{2}$ . **b** Calculated temperature-dependent effective moment  $\mu_{\text{eff}}(T)$  for  $\Delta = 0.018$  eV and SOC  $\lambda = 0.15$  eV. **c** Modified Curie-Weiss fit of RuBr<sub>3</sub> data, taking into account such  $\mu_{\text{eff}}(T)$ . **d** Dependence of best-fit Weiss constants on assumed  $\Delta$ . Vertical dashed line indicates  $\Delta = 0.018$  eV.

for the out-of-plane field, revealing an average CW constant,  $\Theta^{\text{avg}} = \frac{2\Theta^{\parallel} + \Theta^{\perp}}{3}$ , of  $\approx 48$  K. This indicates predominant ferromagnetic (FM) interactions, as they have become established for the magnetic Hamiltonian in RuCl<sub>3</sub> [34–37]. Considering a similar strategy (see ‘Methods’ section), we fit the average susceptibility  $\chi^{\text{avg}}$  of RuBr<sub>3</sub> [25]. However, since the crystal-field parameter  $\Delta$  primarily controls the in-plane vs out-of-plane anisotropy, and for RuBr<sub>3</sub> only powder-averaged data are available, we do not aim at extracting  $\Delta$  by fitting. Instead, we first fix  $\Delta$  using our first-principles calculations, enforcing  $\mu_{\text{eff}}^{\parallel}/\mu_{\text{eff}}^{\perp}(T = 0\text{K}) \propto g_{\parallel}/g_{\perp}$ , where  $g_{\parallel}/g_{\perp}$  are taken from quantum chemistry calculations (see Fig. 5a, discussed below). This leads to  $\Delta = 0.018$  eV. The best CW fit accounting for the implied  $\mu_{\text{eff}}(T, \Delta = 0.018$  eV) (shown in Fig. 2c) yields Weiss constants  $\Theta^{\parallel} \approx 5$  K,  $\Theta^{\perp} \approx 17$  K and  $\Theta^{\text{avg}} \approx 9$  K, which are positive, indicating predominately ferromagnetic interactions for RuBr<sub>3</sub>, as seen before in RuCl<sub>3</sub>. In Fig. 2d we further analyze how the best-fit Weiss constants evolve for other choices of  $\Delta$ . Indeed, for a wide range of reasonable  $\Delta$  around the first-principles value (indicated by the dashed vertical line), the average Weiss constant  $\Theta^{\text{avg}}$  remains positive.

Importantly, for both materials, a standard residual ‘background’ term has to be included in the fitting, which in our

case, depending on the material (RuBr<sub>3</sub> or RuCl<sub>3</sub>) ranges from  $\sim -3.5 \times 10^{-4}$  emu/mol to  $1.5 \times 10^{-4}$ . This is of the same order of magnitude as the corresponding term in RuI<sub>3</sub> ( $\sim 3$  to  $8 \times 10^{-4}$  emu/mol) [26, 27]. Since in the former cases an intrinsic Pauli origin can be excluded, this observation also casts doubts on a metallic interpretation of this term in RuI<sub>3</sub>. Actually, the two available susceptibility measurements on RuI<sub>3</sub> display different behaviors, one nearly temperature-independent [26], and the other [27] showing a Curie-like rise at low temperatures, where a standard CW fit yields  $\mu_{\text{eff}} = 0.53\mu_{\text{B}}$  and  $\Theta_{\text{CW}}^{\text{avg}} = -3$  K [27]. These differences are consistent with our hypothesis that the measured samples consist of magnetic insulating grains surrounded by metallic boundaries. Then, the samples with larger resistivity data [27] hint to larger insulating grains, hence less metallic boundaries are present, leading to the low-temperature Curie-like upturn in the susceptibility, compared to the samples in Ref. 26.

### Electronic and magnetic calculations

In the following we present a comparison of the electronic and magnetic properties of the trihalide RuX<sub>3</sub> family obtained from a combination of density functional theory (DFT) and exact diagonalization of *ab-initio*-derived low-energy models. Details of the calculations are given in the "Methods" section.

Past experience with first-principles calculations for the Ru-based trihalides [4, 7, 38–40] indicates that the magnetic order and, to a considerably lesser extent, metallicity is very fragile, with several closely competing different magnetic phases. The ground states may vary depending on small changes in the crystal structure, on the way in which strong correlations are accounted for, and even on tiny details of the computational protocol. With this in mind, it is imperative to compare the calculated properties across the series, using the exact same computational setup.

For the electronic structure calculations we consider the experimentally reported C2/m [4, 9] and R $\bar{3}$  [41] structures for RuCl<sub>3</sub>, and the suggested R $\bar{3}$  structures for RuBr<sub>3</sub> [25] and RuI<sub>3</sub> [27]. Structural details of the four models are summarized in the Supplementary Information. For RuCl<sub>3</sub>, the R $\bar{3}$  results are shown in Supplementary Information due to very similar results to the C2/m ones.

Figure 3 shows the relativistic density of states (DOS) obtained within GGA+SOC+U as implemented in Wien2k, where a zigzag magnetic configuration with magnetic moments polarized perpendicular to the *ab* plane was considered. For the choice of  $U_{\text{eff}} = U - J$  we take as a reference the *ab initio* estimates for the orbitally-averaged Hubbard on-site ( $U_{\text{avg}}$ ) and Hund's coupling ( $J_{\text{avg}}$ ) as obtained from constrained random-phase approximation (cRPA) calculations (see "Methods" section for calculation details). In contrast to previous cRPA estimates for RuCl<sub>3</sub> [42], our estimates incorporate all five *d* orbitals and extend to the complete Ru-based trihalide family. As shown in Fig. 4a, the effective Hubbard interaction parameters decrease with increasing ligand atomic number from Cl to I, which can be attributed to the more delocalized nature of the Ru *d*

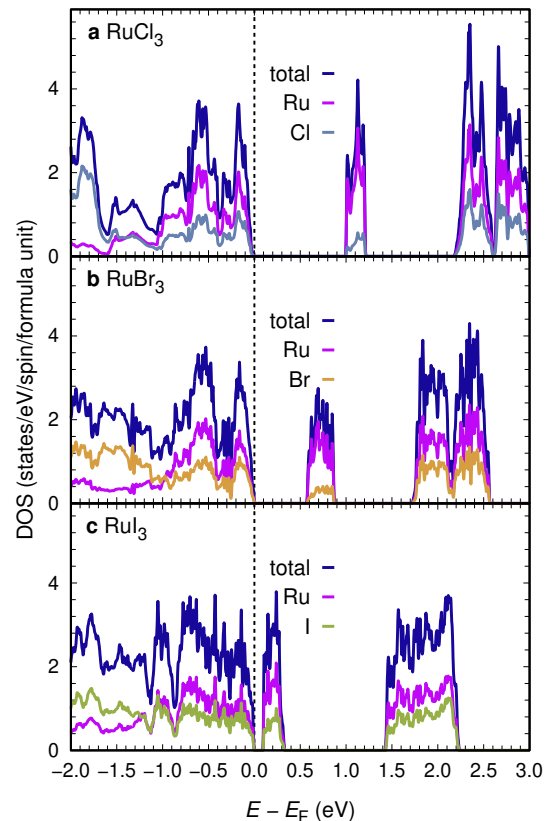


FIG. 3. **Density of states for RuX<sub>3</sub> (X=Cl, Br, I)** Density of states (DOS) for the experimental structures of RuCl<sub>3</sub>, RuBr<sub>3</sub> and RuI<sub>3</sub>, obtained from GGA+SO+U calculations with Wien2k, considering antiferromagnetic zigzag magnetic configurations. For RuCl<sub>3</sub> we employed  $U_{\text{eff}} = 2.7$  eV, for RuBr<sub>3</sub>  $U_{\text{eff}} = 2.1$  eV and for RuI<sub>3</sub>  $U_{\text{eff}} = 1.4$  eV. Shown is also the contribution of Ru and halogen states to the DOS.

orbitals in RuI<sub>3</sub> compared to RuCl<sub>3</sub> when hybridizing with I instead of Cl.

For RuCl<sub>3</sub> a  $U_{\text{eff}} = 2.7$  eV yields both the fundamental and direct gap to be  $\approx 1$  eV (Figure 3a) in agreement with the reported optical gap, apart from the presence of multiplets at 200 meV [43]. We systematically reduced  $U_{\text{eff}}$  to 2.1 eV for RuBr<sub>3</sub> and 1.4 eV for RuI<sub>3</sub> following the trend given by the cRPA results. With these values, RuBr<sub>3</sub> shows a gap of 0.56 eV (Figure 3b), while RuI<sub>3</sub> shows a small gap of 0.1 eV (Figure 3c). The gap closes in RuI<sub>3</sub> when  $U_{\text{eff}}$  is further reduced to 1 eV. These results indicate a spin-orbit assisted Mott insulating state in disorder-free RuI<sub>3</sub> samples, which is on the verge of a metal-insulator transition. Possibly, as discussed above, disorder in the experimental samples could act as effective pressure, and bring the samples closer or over the Mott transition as seen in other Mott insulators [30]. Note that these results hold regardless of the assumed magnetic pattern in the calculations.

In order to analyze the magnetic structure of the RuX<sub>3</sub> compounds, we first consider spin-polarized total energy calculations with VASP in the GGA+SOC+U approxima-



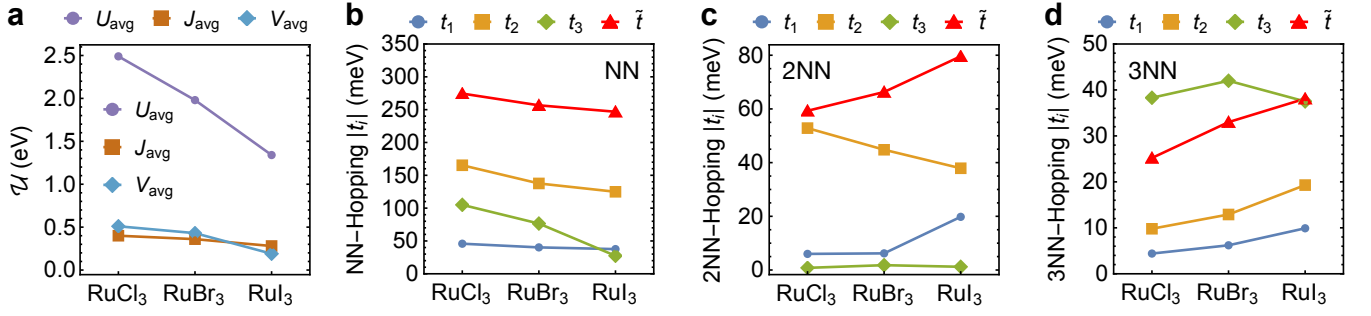


FIG. 4. **Ab-initio-computed multi-orbital Hubbard model parameters across the RuX<sub>3</sub> family.** **a** cRPA results for the orbital-averaged on-site Hubbard interaction ( $U_{\text{avg}}$ ), Hund's coupling ( $J_{\text{avg}}$ ), and the nearest-neighbour  $V_{\text{avg}}$  coupling. **b** Absolute magnitude of hopping parameters  $t_1 = t_{(yz,yz)}$ ,  $t_2 = t_{(xz,yz)}$ ,  $t_3 = t_{(xy,xy)}$ , and  $\tilde{t} = t_{(xy,z^2)}$  on nearest-neighbor (NN), second-neighbor (2NN) and third-neighbor (3NN) Z-bonds.

tion (see also ‘Methods’). Detailed results are listed in the Supplementary Information. For RuCl<sub>3</sub>, the calculated energy of the ferromagnetic state  $E_{\text{FM}}$  is very competitive with the energy of the experimentally observed zigzag ordered state  $E_{\text{ZZ}}$ :  $E_{\text{ZZ}} - E_{\text{FM}} \approx 2 \text{ meV/Ru}$ . This observation is consistent with the evidence for a metastable ferromagnetic state in RuCl<sub>3</sub> [37, 44]. Correspondingly, in our effective pseudospin model of RuCl<sub>3</sub> discussed below, classically, the energy of the ferromagnet is below that of zigzag, and only by including quantum fluctuations the zigzag ground state is recovered (as in, e.g., Ref. [37]). For RuBr<sub>3</sub> we find an energy minimum for the zigzag ordering in agreement with the experiment. Interestingly, for RuI<sub>3</sub> Néel and zigzag orders are energetically almost degenerate  $E_{\text{Néel}} - E_{\text{ZZ}} \approx 1 \text{ meV/Ru}$ , with the rest of magnetic orders we scanned being energetically rather close. All orders show very small and varying magnetic moments for Ru. These results hint to a magnetic frustration.

We proceed with the derivation of magnetic exchange models. In the first place, the magnetic Hamiltonian of RuBr<sub>3</sub> has been suggested to be closer to the pure Kitaev limit than in RuCl<sub>3</sub> [25], and, secondly, with our proposed scenario of a Mott insulating state for RuI<sub>3</sub>, the question of its magnetic properties is open. To investigate these issues from first principles, we derive via the *ab-initio* projED method [45] the pseudospin models  $\mathcal{H}_{\text{eff}} = \sum_{ij} \mathbf{S}_i \cdot \mathbb{J}_{ij} \cdot \mathbf{S}_j$  of the three RuX<sub>3</sub> compounds. Here,  $\mathbf{S}$  stands for the relativistic pseudospin  $j_{\text{eff}} = 1/2$  moment [2].

In the conventional parametrization of Kitaev materials, the exchange matrix  $\mathbb{J}_{ij}$  in R $\bar{3}$  symmetry on a nearest-neighbor Z<sub>1</sub>-bond (defined in Fig. 1) follows the form

$$\mathbb{J}_{ij} = \begin{pmatrix} J_1 + \nu_1 & \Gamma_1 & \Gamma'_1 + \eta_1 \\ \Gamma_1 & J_1 - \nu_1 & \Gamma'_1 - \eta_1 \\ \Gamma'_1 + \eta_1 & \Gamma'_1 - \eta_1 & J_1 + K_1 \end{pmatrix}, \quad (1)$$

with the isotropic Heisenberg exchange  $J_1$ , the bond-dependent anisotropic Kitaev exchange  $K_1$ , the bond-dependent off-diagonal exchange terms  $\Gamma_1$  and  $\Gamma'_1$  and correction terms  $\eta_1$  and  $\nu_1$ . The latter correction terms are found to be small in our calculated Hamiltonians, and are neglected in what follows. The exchange matrices on X-

and Y-bonds follow by respective  $C_3$  rotations about the out-of-plane axis ([111] in pseudospin coordinates). Analogously follow the definitions for second and third neighbor exchange terms (or see, e.g., Ref. 8).

Using  $U_{\text{avg}}$  and  $J_{\text{avg}}$  from cRPA (Fig. 4a), the complex hopping parameters extracted from full-relativistic DFT (magnitudes shown in Fig. 4b,c,d) and the projED method, we extracted the exchange constants shown in Fig. 5b,c,d.

Evaluating the magnetic interactions of the complete RuX<sub>3</sub> family, we find a nearest-neighbor ferromagnetic Kitaev interaction  $K_1$  to be the dominant in all three compounds. Additionally, a subdominant ferromagnetic nearest-neighbor Heisenberg exchange  $J_1$  is present, which is, however, almost vanishing for the iodine case. The symmetric off-diagonal  $\Gamma_1$  interaction is of similar magnitude as  $J_1$ , changing sign going from Cl and Br to I.  $\Gamma'_1$ , often neglected in the RuCl<sub>3</sub> analysis, may become rather important, particularly for RuI<sub>3</sub>. Further-neighbor interactions are generally smaller than their nearest-neighbor counterparts for all three systems, but increase for larger ligand atomic number and may play, especially in RuI<sub>3</sub>, an important role.

That the anisotropic interactions do not monotonically increase with stronger spin-orbit coupling of halogen elements can be related to the SOC source. In the original Jackeli-Khaliullin mechanism [2], the heavy magnetic ions are solely responsible for SOC effects, which can be well described within the SOC atomic limit. In the case of RuBr<sub>3</sub> and RuI<sub>3</sub>, however, ligand SOC starts to play an important role. To evaluate the interplay of these two SOC sources, we extracted *ab initio* values for the RuX<sub>3</sub> materials and compared them to the SOC atomic limit (see Supplementary Information). We find that in these compounds SOC effects from magnetic ions and ligands do not enhance each other, but do compete. This leads to the observed inhomogeneous behavior of the magnetic anisotropic terms in Fig. 5 as a function of ligand atomic number. Another consequence of this breakdown of the SOC atomic limit is that the established analytic perturbation theory expressions [2, 6, 8] become unjustified in Kitaev materials where SOC arises from both the metal and the ligand elements. RuBr<sub>3</sub> and RuI<sub>3</sub> are therefore cases where more general approaches, like

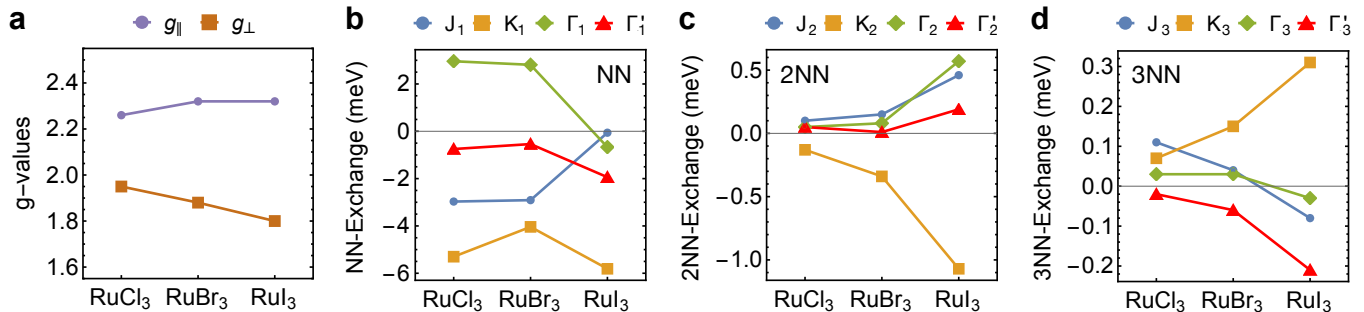


FIG. 5. **Ab-initio computed pseudospin models across the RuX<sub>3</sub> family.** **a** Quantum chemistry results for local gyromagnetic  $g$ -tensor components  $g_{\parallel}$  (in-plane) and  $g_{\perp}$  (out-of-plane). **b-d** projED results for the magnetic exchange couplings on nearest-neighbor (NN), second-neighbor (2NN) and third-neighbor (3NN) bonds. Tabular form of all values is given in the Supplementary Information.

ours, are indispensable. Another approach would be perturbation theory taking into account ligand orbitals, as recently derived for the  $S = 3/2$  material CrI<sub>3</sub> [46].

Along the halogen series Cl-Br-I we observe a decrease for nearest-neighbor couplings (Fig. 5b) and an overall increase in magnitude for second and third neighbors (Fig. 5c,d). This can be understood by consideration of the ligand-metal ( $p$ - $d$ ) hybridization. We quantify the hybridization strength by integrating the DFT(GGA) density of states (DOS) with Ru  $4d$  orbital character in the energy window dominated by the ligand  $p$  orbitals (between  $-7$  eV and  $-1.05$  eV). In spite of respective larger Ru-Ru distances, this can be related to the magnetic exchange by consideration of the *ab initio* hopping parameters between Wannier  $d$  orbitals. As also pointed out in Ref. 39, in spite of the stronger hybridization the nearest-neighbor hopping parameters are reduced for heavier ligands, illustrated in Fig. 4b. This is reflected in the magnetic exchange parameters (Fig. 5b) in an overall reduced magnitude in the nearest-neighbor parameters. In contrast, the second and third neighbors show a very different dependence on the halogen element. From the dominant further-neighbor hoppings (Fig. 4c,d), the hoppings show an overall tendency to increase, with few exceptions. Certain further-neighbor magnetic exchange parameters, depending on their relation to the individual hopping parameters, become therefore increasingly important for RuBr<sub>3</sub> and especially for the magnetic properties of RuI<sub>3</sub>. Finally, we also computed the gyromagnetic  $g$ -tensor for the RuX<sub>3</sub> family from first principles, in order to relate the pseudospin  $\mathbf{S}$  of the effective Hamiltonian to the magnetic moment  $\mathbf{M} = \mu_B \mathbb{G} \cdot \mathbf{S}$ . The  $g$ -tensor can be approximately characterized by two components, the value parallel to the honeycomb plane,  $g_{\parallel}$ , and the one perpendicular to it,  $g_{\perp}$ , which are shown in Fig. 5a. We consistently find  $g_{\parallel} > g_{\perp}$  for the whole family, promoting a stronger Zeeman term for in-plane fields.

We now discuss the ramifications of the derived magnetic models for the magnetism in these materials.

For RuCl<sub>3</sub>, we can compare our result to a vast available literature of models that have been shown to reproduce various experimental observations. Indeed, the model presented

RuX <sub>3</sub>	RuCl <sub>3</sub>	RuBr <sub>3</sub>	RuI <sub>3</sub>
$\Theta_{CW}^{avg}$	+39.1 K	+35.6 K	+15.4 K
GS	Zigzag	Zigzag	QSL?
$\phi_M$	90°	90°	
$\theta_M$	34.4°	32.4°	

TABLE 2. **Properties of derived pseudospin models.**  $\Theta_{CW}^{avg}$  is the powder-averaged Weiss temperature of each model. 'GS' refers to the ground state computed by exact diagonalization, and the angles of the magnetic moment  $\phi_M, \theta_M$  are defined according to Fig. 1b.

here in Fig. 5, derived completely from first principles without adjustments or external parameters, is remarkably close to some well-benchmarked recent models [19, 37, 38], and is therefore expected to also describe the material quite well. As we apply the same *ab-initio* setup for the new members of the RuX<sub>3</sub> family, we expect our models to be reliable for them too.

The direction-averaged Weiss constant ( $\Theta_{CW}^{avg}$  in Table 2) is predicted to be positive across the RuX<sub>3</sub> family, characteristic of ferromagnetic exchange interactions. This is in line with our analysis of the experimental magnetic susceptibilities of RuCl<sub>3</sub> and RuBr<sub>3</sub> above (Fig. 2). While in RuCl<sub>3</sub> and RuBr<sub>3</sub> a large FM contribution to the Weiss constant comes from a significant FM nearest-neighbor Heisenberg interaction  $J_1$ , this interaction nearly vanishes for RuI<sub>3</sub> (Fig. 5b), leading to a smaller Weiss constant. Furthermore, the small  $J_1$  in RuI<sub>3</sub> renders the nearest-neighbor interactions to be extremely anisotropic, with a dominant Kitaev interaction  $K_1$ . While at first glance this might suggest a spin-liquid ground state in RuI<sub>3</sub>, the increased strength of the further-neighbor interactions in RuI<sub>3</sub> (see, e.g.,  $J_2, K_2$  in Fig. 5c) also needs to be considered [47].

To find the magnetic ground state properties, we perform exact diagonalization (ED) calculations of the derived  $j_{eff} = 1/2$  models on the 24-site cluster shown in Fig. 6a. In Table 2 and Fig. 6b we summarize the encountered ground states, i.e. zigzag for RuCl<sub>3</sub> and RuBr<sub>3</sub>, and possibly a quantum spin liquid (QSL) in RuI<sub>3</sub>. This is discussed in detail

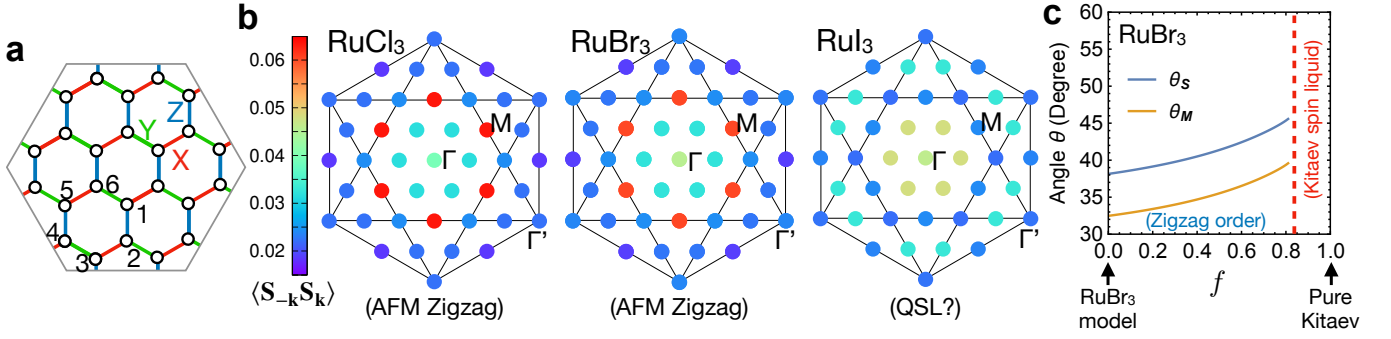


FIG. 6. **Exact diagonalization of  $\text{RuX}_3$  pseudospin models.** **a** Employed periodic cluster. Labeled sites 1, . . . , 6 define the Kitaev plaquette operator  $W_p = 2^6 S_1^x S_2^y S_3^z S_4^x S_5^y S_6^z$ . **b** Static spin structure factor in reciprocal space. Inner (outer) hexagon mark the edge of the first (third) Brillouin Zone. High-symmetry  $k$ -points  $\Gamma, M, \Gamma'$  are labeled. Color scale is the same for all three plots. **c** Out-of-plane angle  $\theta_S$  ( $\theta_M$ ) of the pseudospin (magnetic moment) within the zigzag phase when tuning from the  $\text{RuBr}_3$  model ( $f = 0$ ) towards the pure Kitaev model ( $f = 1$ ). Dashed vertical line indicates phase transition to the Kitaev spin liquid, identified by a peak in  $-\partial^2 E / \partial f^2$ .

below.

For  $\text{RuCl}_3$ , the model in Fig. 5 (as well as the  $R\bar{3}$  model discussed in the Supplementary Information) yields zigzag AFM order, identifiable by a maximum at  $\mathbf{k} = M$  in the static spin structure factor, shown in Fig. 6b. The computed ordered magnetic moment direction (see ‘Methods’ section), parametrized by  $\theta$  and  $\phi$  in Table 2 (compare Fig. 1b), is found to be tilted by  $\theta_M \approx 34^\circ$  out of the plane, in excellent agreement with the recent experiment, where  $\theta_M = 32 \pm 3^\circ$  [36] was reported. Interestingly, on the classical level, the ferromagnetic state is lower in energy than the zigzag state, meaning that the latter only becomes the ground state through quantum fluctuations, as discussed also in Ref. [37].

We will now focus on the recently synthesized compounds, starting with  $\text{RuBr}_3$ . The static spin structure factor for the  $\text{RuBr}_3$  model of Fig. 5 is shown in Fig. 6b, indicating also a zigzag AFM order ( $\mathbf{k} = M$  and  $C_6$ -rotated vectors), in agreement with experiment [25]. However, the calculated tilt angle of the magnetic moment,  $\theta_M = 32^\circ$ , is more in line with  $\text{RuCl}_3$  than with the reported measured  $\theta_M = 64^\circ$  of  $\text{RuBr}_3$  [25]. The authors of Ref. 25 argued that this anomalously large tilt angle indicates an exceptionally strong relative Kitaev coupling, *i.e.*, larger  $|K_1/J_1|$  and  $|K_1/\Gamma_1|$  compared to  $\text{RuCl}_3$ . To investigate to what extent a closer proximity to the pure Kitaev model could produce such high tilt angles, we take our  $\text{RuBr}_3$  Hamiltonian of Fig. 5 as a starting point and tune towards the pure Kitaev model, where  $K_1$  is the only non-zero coupling. This is done by multiplying every exchange coupling except  $K_1$  by  $(1 - f)$  and sweeping  $f$  from 0 to 1. As shown in Fig. 6c, the moment indeed rotates further away from the honeycomb plane upon moving towards the pure Kitaev model, however even right before the transition to the Kitaev spin liquid (indicated by the vertical dashed line),  $\theta_S$  does not exceed  $46^\circ$ .  $\theta_M = \arccos\left(\frac{\cos \theta_S}{\sqrt{g_{\parallel}^2 \cos^2 \theta_S + g_{\perp}^2 \sin^2 \theta_S}}\right)$ , which is to be compared to the neutron diffraction experiment, is even smaller due to the anisotropy  $g_{\parallel} > g_{\perp}$  in our calcu-

lated  $g$ -tensor (Fig. 5a). A reconciliation with the reported  $\theta_M = 64^\circ$  would therefore require quite drastic changes to the  $g$ -tensor anisotropy and/or the exchange parameters. While in the whole  $J_1$ - $K_1$ - $\Gamma_1$  parameter space with  $\Gamma_1 > 0$ , no angles of  $\theta_S$  beyond  $\sim 40^\circ$  are expected in the zigzag phase [48], significant *negative*  $\Gamma_1 < 0$  can in principle lead to  $\theta_S$  beyond  $60^\circ$  [49]. However such terms seem incompatible with the *ab-initio* results and would likely need strong distortions from the present considered  $\text{RuBr}_3$  crystal structure to be realized.

More distinct from the other two compounds are our results for  $\text{RuI}_3$ . As discussed above, in our GGA+SOC+U calculations we find a very flat energy landscape of competitive magnetic configurations, indicative of strong magnetic frustration. Fittingly, the ground state from exact diagonalization of the present exchange model does not show a dominant ordering wave vector in the spin structure factor, see Fig. 6b. Although this is a signature generally associated with quantum spin liquid (QSL) states, we note that in the present model, the Kitaev  $\mathbb{Z}_2$  flux operator yields  $\langle W_p \rangle = 2^6 \langle S_1^x S_2^y S_3^z S_4^x S_5^y S_6^z \rangle \approx 0.29$  (site indices refer to Fig. 6a). While this is clearly elevated compared to classical collinear states, where  $\langle W_p \rangle$  is restricted to  $|\langle W_p \rangle| \leq \frac{1}{2^7} < 0.04$ , it is still significantly below the value of the pure unperturbed Kitaev spin liquid, where  $\langle W_p \rangle = 1$  [1]. Hence, if the ground state constitutes a QSL state, it is presumably not the  $\mathbb{Z}_2$  Kitaev spin liquid. The precise nature of the encountered magnetically disordered state might be interesting for future studies. It appears to be stabilized by the further-neighbor interactions, as we find a clear ferromagnetic ground state when omitting the second- and third-neighbor interactions in the present model. While a QSL scenario for our full  $\text{RuI}_3$  model is compelling, we note that finite-size effects in our calculation could play a role. In particular, the finite-size cluster could be incompatible with the supposed correct ordering wave vector of the model, *e.g.* in case of an incommensurate ordering vector.

## Conclusions and outlook

To summarize, we have presented a comparative analysis of the electronic and magnetic properties of the Ru-based trihalide family, including the recently synthesized  $\text{RuBr}_3$  and  $\text{RuI}_3$ , by combining state-of-the-art *ab initio* microscopic modelling with analysis of reported resistivity, specific heat and magnetic susceptibility data. The evolution of the magnetic order and Mott-Hubbard correlations along the halogen series, as well as possible role of disorder, have been a central part of our study. We conclude that:

1. All three ideal compounds are spin-orbit-assisted Mott insulators, but their fundamental gap decreases with higher ligand atomic number,  $\text{Cl} \rightarrow \text{Br} \rightarrow \text{I}$ , with  $\text{RuI}_3$  coming rather close to a metal-insulator transition.
2. From DFT total-energy calculations, in ideal, pristine crystals the zigzag magnetic order is even more stable in  $\text{RuBr}_3$  than in  $\text{RuCl}_3$ , while  $\text{RuI}_3$  shows significant magnetic frustration. Our *ab-initio* extracted low-energy models predict  $\text{RuI}_3$  to feature either an incommensurate magnetic ordered state or a quantum spin liquid, which, interestingly, is possibly of a different kind to the  $\mathbb{Z}_2$  Kitaev spin liquid.
3. A number of reported experimental observations seem to be adversely affected by the sample quality, in particular by dirty grain boundaries. In fact, most of the observations in  $\text{RuI}_3$  can be reconciled with theory by assuming insulating grains surrounded by (bad) metallic boundaries. The experimental evidence is consistent with a ‘dirty’ insulator, or a bad metal. Disorder would favor either of these.
4. In all three systems the dominant nearest-neighbor interaction is FM Kitaev  $K_1$ , with a subdominant FM Heisenberg Interaction  $J_1$ , that nearly vanishes for  $\text{RuI}_3$ . We observe a non-monotonous behavior of the magnetic anisotropic terms as a function of ligand atomic number that we trace back to a competition of the SOC effects from magnetic ions and ligands.
5.  $\text{RuBr}_3$  has predominantly ferromagnetic interactions, in contrast to what is suggested by standard Curie-Weiss analysis [25]. Such interactions are consistent with the experimental susceptibility when taking into account high-temperature SOC effects. Our *ab-initio* magnetic model predicts zigzag order in agreement with experiment, with a tilting angle of  $\theta_M = 32^\circ$  for the magnetic moments, similar to  $\text{RuCl}_3$ , but in contradiction to the reported  $\theta_M = 64^\circ$  [25]. We showed that such a large angle cannot be simply explained by proximity to the pure Kitaev model, but would require quite drastic changes to the exchange parameters, such as sizeable negative  $\Gamma_1 < 0$ . Those would necessitate strong distortions on the reported  $\text{RuBr}_3$  crystal structures.

Answering the question posed in the title, our results and analysis strongly suggest that the ideal  $\text{RuCl}_3$ ,  $\text{RuBr}_3$  and

$\text{RuI}_3$  compounds constitute a family of three Mott-insulating *siblings*. The challenging task of getting better samples will hopefully help resolve the open issues.

## METHODS

### Modified Curie-Weiss fit of $\text{RuBr}_3$

We fit the experimental average susceptibility of Ref. 25 with four fitting parameters  $\chi_0^\perp, \chi_0^\parallel, \Theta^\perp, \Theta^\parallel$  using the modified Curie-Weiss formula

$$\chi^{\text{avg}}(T) \approx \frac{2}{3} \left( \chi_0^\parallel + \frac{C^\parallel(T)}{T - \Theta^\parallel} \right) + \frac{1}{3} \left( \chi_0^\perp + \frac{C^\perp(T)}{T - \Theta^\perp} \right), \quad (2)$$

where  $\Theta^\parallel, \Theta^\perp$  are the Weiss constants and  $C^\alpha(T) \propto [\mu_{\text{eff}}^\alpha(T, \Delta)]^2$  is determined through  $\Delta$  as described in Ref. 33. Superscripts  $\parallel$  and  $\perp$  indicate the in- and out-of-honeycomb-plane direction respectively. The susceptibility is fitted over the temperature range 150 – 300 K and SOC strength  $\lambda = 0.15$  eV is taken.

### DFT calculations

To make sure that the calculated features within density functional theory are robust with respect to the choice of the basis set, we have tested the results using two different methods: the projector augmented wave method [50, 51] as implemented in the VASP code [52, 53], and the full potential linearized augmented plane-wave (LAPW) basis as implemented in Wien2k [54]. Throughout the paper we have used the Generalized Gradient Approximation (GGA [55]) to the exchange-correlation functional. Hubbard correlation effects were included on a mean field level in the rotationally invariant implementation of the GGA+U method [56]. All calculations included spin-orbit coupling (SOC) effects. For VASP we used the Ru\_pv pseudopotential, treating Ru *p* states as valence, and the standard pseudopotentials for the halogens. The  $\Gamma$ -centered  $8 \times 8 \times 8$  mesh in the nonmagnetic rhombohedral Brillouin zone was used, or the correspondingly scaled meshes for other structures. The energy cut-off was 350 eV, and the energy convergence criterion  $1 \times 10^{-08}$  eV. For each type of magnetic order a number of collinear starting configurations with randomly selected Néel vectors were used, and the lowest-energy result was selected as the ground state. Individual results can be found in the Supplementary Information. For Wien2k we chose the plane-wave cutoff  $K_{\text{max}}$  corresponding to  $\text{RK}_{\text{max}} = 8$  and a  $\mathbf{k}$  mesh of  $8 \times 8 \times 2$  for the  $\text{R}\bar{3}$  structure in the hexagonal Brillouin zone and  $8 \times 4 \times 6$  in the first Brillouin zone of the conventional unit cell for the  $C/2m$  structure. The density of states are calculated using a  $\mathbf{k}$  mesh of  $12 \times 12 \times 3$  for the  $\text{R}\bar{3}$  structure and  $12 \times 6 \times 9$  for the  $C/2m$  structure. The zigzag configurations are constructed using a conventional cell of the  $C/2m$  structure for  $\text{RuCl}_3$  while a  $1 \times 2 \times 1$  supercell of the  $\text{R}\bar{3}$  structures for  $\text{RuBr}_3$  and  $\text{RuCl}_3$ .



## cRPA calculations

In order to obtain *ab-initio* estimates for the effective Coulomb interaction for the Ru-trihalide family, we employed the constrained random-phase approximation (cRPA) [57, 58], as implemented in the FHI-gap code [59], based on the Wien2K electronic structure. The low-energy limit of the screened interaction was projected on the five Ru  $d$  orbitals, where screening processes in the same window were excluded. Convergence with respect to the discretization of the Brillouin zone and energy cutoff was ensured.

## DFT-based derivation of magnetic models

To derive bilinear exchange parameters for each material, we employed the projED method [45], which consists of two steps. First, complex *ab-initio* hopping parameters between the ruthenium ions are estimated with projective Wannier functions [60] applied on full relativistic FPLO [61] calculations on a  $12 \times 12 \times 12$   $\mathbf{k}$  mesh. This allows to construct an effective electronic model  $\mathcal{H}_{\text{tot}} = \mathcal{H}_{\text{hop}} + \mathcal{H}_U$ , where the complex *ab-initio* hopping parameters enter the kinetic term  $\mathcal{H}_{\text{hop}} = \sum_{ij\alpha\beta} \sum_{\sigma\sigma'} t_{i\alpha,j\beta}^{\sigma\sigma'} c_{i\alpha\sigma}^\dagger c_{j\beta\sigma'}$  and the cRPA effective Coulomb interaction parameters enter the two-particle term  $\mathcal{H}_U = \sum_{i\alpha\beta\gamma\delta} \sum_{\sigma\sigma'} U_{i\alpha\beta\gamma\delta}^{\sigma\sigma'} c_{i\alpha\sigma}^\dagger c_{i\beta\sigma'}^\dagger c_{i\delta\sigma} c_{i\gamma\sigma}$ . Second, the effective spin Hamiltonian  $\mathcal{H}_{\text{eff}}$  is extracted from the electronic model via exact diagonalization (ED) and projection of the resulting energy spectrum onto the low-energy subspace, mapped onto pseudo-spin operator representation in the  $j_{\text{eff}}$  picture with the projection operator  $\mathbb{P}$ :  $\mathcal{H}_{\text{eff}} = \mathbb{P}\mathcal{H}_{\text{tot}}\mathbb{P} = \sum_{ij} \mathbf{S}_i \mathbb{J}_{ij} \mathbf{S}_j$ .

Note that for RuCl<sub>3</sub> the exchange constants slightly differ from previously calculated values by some of the authors [8, 38]. The reason for this lies in the following details of the calculation setup: (i) first principles input parameters  $U_{\text{avg}}$  and  $J_{\text{avg}}$  from cRPA in contrast to previous choices, (ii) consideration of all five  $4d$  ruthenium orbitals with the cost of restriction onto two-site clusters, (iii) SOC effects from both Ru<sup>3+</sup> and ligands considered through complex hopping parameters in contrast to the atomic limit, and (iv) consideration of the experimental crystal structure in contrast to relaxed ambient pressure structure as it was done in Ref. 38.

For the calculation of the gyromagnetic  $g$ -tensor, we considered [RuX<sub>6</sub>]<sup>3-</sup> molecules within the quantum chemistry ORCA 3.03 package [62, 63] with the functional TPSSh, basis set def2-TZVP and complete active space for the  $d$  orbitals CAS(5,5).

## Exact diagonalization

Exact diagonalization calculations of the  $j_{\text{eff}} = 1/2$  models were performed on the 24-site cluster shown in Fig. 6a. To identify possible magnetic ordering, we analyze the static spin structure factor  $\sum_{\mu=x,y,z} \langle S_{-\mathbf{k}}^\mu S_{\mathbf{k}}^\mu \rangle$ . For the ordered moment direction, we compute the eigenvector with maximal eigenvalue of the correlation matrix  $(\langle S_{-\mathbf{k}}^\mu S_{\mathbf{k}}^\nu \rangle)_{\mu,\nu}$  ( $\mu, \nu \in \{x, y, z\}$ ) at the ordering wave vector  $\mathbf{k} = \mathbf{Q}$ . This eigenvector then represents the ordered *pseudospin* direction  $\mathbf{S}$  [49], which relates to the magnetic moment direction  $\mathbf{M} \propto \mathbb{G} \cdot \mathbf{S}$ , as measured by neutron diffraction, via the anisotropic  $g$ -tensor  $\mathbb{G}$ .

## ACKNOWLEDGMENTS

We thank Stephen M. Winter, Robert J. Cava, Yoshinori Imai, and Elena Gati for discussions and Yoshinori Imai for sharing the structural information of RuBr<sub>3</sub> with us before publication. R.V., A.R., K.R. and D.A.S.K. acknowledge support by the Deutsche Forschungsgemeinschaft (DFG, German Research Foundation) for funding through Project No. 411289067 (VA117/15-1) and TRR 288 — 422213477 (project A05). Y.L. acknowledges support by National Natural Science Foundation of China (Grant No. 12004296) and China Postdoctoral Science Foundation (Grant No. 2019M660249). I.I.M. acknowledges support from the U.S. Department of Energy through the grant #DE-SC0021089. R.V. and I.I.M. thank the Wilhelm und Else Heraeus Stiftung for financial support.

## COMPETING INTERESTS

We declare no competing interests.

## AUTHOR CONTRIBUTIONS

R.V. conceived and supervised the project. Density functional theory calculations were performed by K.R., A.R., Y.L., I.I.M., cRPA calculations by S.B., projED calculations by K.R., and calculations on magnetic models by D.A.S.K. All authors contributed to the manuscript.

## SUPPLEMENTARY INFORMATION

The online version contains supplementary material available at ...

- 
- [1] Kitaev, A. Anyons in an exactly solved model and beyond. *Ann. Phys.* **321**, 2–111 (2006).
  - [2] Jackeli, G. & Khaliullin, G. Mott insulators in the strong spin-orbit coupling limit: From Heisenberg to a quantum compass and Kitaev models. *Phys. Rev. Lett.* **102**, 017205 (2009).
  - [3] Plumb, K. W. *et al.*  $\alpha$ -RuCl<sub>3</sub>: A spin-orbit assisted Mott insulator on a honeycomb lattice. *Phys. Rev. B* **90**, 041112 (2014).
  - [4] Johnson, R. D. *et al.* Monoclinic crystal structure of  $\alpha$ -RuCl<sub>3</sub> and the zigzag antiferromagnetic ground state. *Phys. Rev. B* **92**, 235119 (2015).
  - [5] Zhou, X. *et al.* Angle-resolved photoemission study of the Kitaev candidate  $\alpha$ -RuCl<sub>3</sub>. *Phys. Rev. B* **94**, 161106 (2016).
  - [6] Rau, J. G., Lee, E. K.-H. & Kee, H.-Y. Generic spin model for the honeycomb iridates beyond the Kitaev limit. *Phys. Rev. Lett.* **112**, 077204 (2014).

- [7] Kim, H.-S. & Kee, H.-Y. Crystal structure and magnetism in  $\alpha$ -RuCl<sub>3</sub>: An ab initio study. *Phys. Rev. B* **93**, 155143 (2016).
- [8] Winter, S. M., Li, Y., Jeschke, H. O. & Valentí, R. Challenges in design of Kitaev materials: Magnetic interactions from competing energy scales. *Phys. Rev. B* **93**, 214431 (2016).
- [9] Cao, H. B. *et al.* Low-temperature crystal and magnetic structure of  $\alpha$ -RuCl<sub>3</sub>. *Phys. Rev. B* **93**, 134423 (2016).
- [10] Banerjee, A. *et al.* Neutron scattering in the proximate quantum spin liquid  $\alpha$ -RuCl<sub>3</sub>. *Science* **356**, 1055–1059 (2017).
- [11] Sandilands, L. J., Tian, Y., Plumb, K. W., Kim, Y.-J. & Burch, K. S. Scattering continuum and possible fractionalized excitations in  $\alpha$ -RuCl<sub>3</sub>. *Phys. Rev. Lett.* **114**, 147201 (2015).
- [12] Nasu, J., Knolle, J., Kovrizhin, D. L., Motome, Y. & Moessner, R. Fermionic response from fractionalization in an insulating two-dimensional magnet. *Nat. Phys.* **12**, 912–915 (2016).
- [13] Do, S.-H. *et al.* Majorana fermions in the Kitaev quantum spin system  $\alpha$ -RuCl<sub>3</sub>. *Nat. Phys.* **13**, 1079–1084 (2017).
- [14] Widmann, S. *et al.* Thermodynamic evidence of fractionalized excitations in  $\alpha$ -RuCl<sub>3</sub>. *Phys. Rev. B* **99**, 094415 (2019).
- [15] Sears, J. A., Zhao, Y., Xu, Z., Lynn, J. W. & Kim, Y.-J. Phase diagram of  $\alpha$ -RuCl<sub>3</sub> in an in-plane magnetic field. *Phys. Rev. B* **95**, 180411 (2017).
- [16] Banerjee, A. *et al.* Excitations in the field-induced quantum spin liquid state of  $\alpha$ -RuCl<sub>3</sub>. *npj Quantum Mater.* **3**, 8 (2018).
- [17] Kasahara, Y. *et al.* Majorana quantization and half-integer thermal quantum Hall effect in a Kitaev spin liquid. *Nature* **559**, 227–231 (2018).
- [18] Hentrich, R. *et al.* Unusual phonon heat transport in  $\alpha$ -RuCl<sub>3</sub>: Strong spin-phonon scattering and field-induced spin gap. *Phys. Rev. Lett.* **120**, 117204 (2018).
- [19] Winter, S. M. *et al.* Breakdown of magnons in a strongly spin-orbital coupled magnet. *Nat. Commun.* **8**, 1152 (2017).
- [20] Hentrich, R. *et al.* High-field thermal transport properties of the Kitaev quantum magnet  $\alpha$ -RuCl<sub>3</sub>: Evidence for low-energy excitations beyond the critical field. *Phys. Rev. B* **102**, 235155 (2020).
- [21] Sahasrabudhe, A. *et al.* High-field quantum disordered state in  $\alpha$ -RuCl<sub>3</sub>: Spin flips, bound states, and multiparticle continuum. *Phys. Rev. B* **101**, 140410(R) (2020).
- [22] Chern, L. E., Zhang, E. Z. & Kim, Y. B. Sign structure of thermal Hall conductivity and topological magnons for in-plane field polarized Kitaev magnets. *Phys. Rev. Lett.* **126**, 147201 (2021).
- [23] Czajka, P. *et al.* Oscillations of the thermal conductivity in the spin-liquid state of  $\alpha$ -RuCl<sub>3</sub>. *Nat. Phys.* **17**, 915–919 (2021).
- [24] Lefrançois, É. *et al.* Evidence of a phonon Hall effect in the Kitaev spin liquid candidate  $\alpha$ -RuCl<sub>3</sub>. *Phys. Rev. X* **12**, 021025 (2022).
- [25] Imai, Y. *et al.* Zigzag magnetic order in the Kitaev spin-liquid candidate material RuBr<sub>3</sub> with a honeycomb lattice. *Phys. Rev. B* **105**, L041112 (2022).
- [26] Nawa, K. *et al.* Strongly electron-correlated semimetal RuI<sub>3</sub> with a layered honeycomb structure. *J. Phys. Soc. Japan* **90**, 123703 (2021).
- [27] Ni, D., Gui, X., Powderly, K. M. & Cava, R. J. Honeycomb-structure RuI<sub>3</sub>, a new quantum material related to  $\alpha$ -RuCl<sub>3</sub>. *Adv. Mater.* **34**, 2106831 (2022).
- [28] Jaramillo, R., Ha, S. D., Silevitch, D. M. & Ramanathan, S. Origins of bad-metal conductivity and the insulator–metal transition in the rare-earth nickelates. *Nat. Phys.* **10**, 304–307 (2014).
- [29] Little, A. *et al.* Antiferromagnetic resonance and terahertz continuum in  $\alpha$ -RuCl<sub>3</sub>. *Phys. Rev. Lett.* **119**, 227201 (2017).
- [30] Gati, E. *et al.* Effects of disorder on the pressure-induced Mott transition in  $\kappa$ -(BEDT-TTF)<sub>2</sub>Cu[N(CN)<sub>2</sub>]Cl. *Crystals* **8**, 38 (2018).
- [31] Tanaka, O. *et al.* Thermodynamic evidence for a field-angle-dependent Majorana gap in a Kitaev spin liquid. *Nat. Phys.* **18**, 429–435 (2022).
- [32] Sears, J. A. *et al.* Magnetic order in  $\alpha$ -RuCl<sub>3</sub>: A honeycomb-lattice quantum magnet with strong spin-orbit coupling. *Phys. Rev. B* **91**, 144420 (2015).
- [33] Li, Y., Winter, S. M., Kaib, D. A. S., Riedl, K. & Valentí, R. Modified Curie-Weiss law for  $j_{\text{eff}}$  magnets. *Phys. Rev. B* **103**, L220408 (2021).
- [34] Winter, S. M. *et al.* Models and materials for generalized Kitaev magnetism. *J. Condens. Matter Phys.* **29**, 493002 (2017).
- [35] Laurell, P. & Okamoto, S. Dynamical and thermal magnetic properties of the Kitaev spin liquid candidate  $\alpha$ -RuCl<sub>3</sub>. *npj Quantum Mater.* **5**, 2 (2020).
- [36] Sears, J. A. *et al.* Ferromagnetic Kitaev interaction and the origin of large magnetic anisotropy in  $\alpha$ -RuCl<sub>3</sub>. *Nat. Phys.* **16**, 837–840 (2020).
- [37] Suzuki, H. *et al.* Proximate ferromagnetic state in the Kitaev model material  $\alpha$ -RuCl<sub>3</sub>. *Nat. Commun.* **12**, 4512 (2021).
- [38] Kaib, D. A. S., Biswas, S., Riedl, K., Winter, S. M. & Valentí, R. Magnetoelastic coupling and effects of uniaxial strain in  $\alpha$ -RuCl<sub>3</sub> from first principles. *Phys. Rev. B* **103**, L140402 (2021).
- [39] Kim, H.-S. Spin-orbit-entangled nature of magnetic moments and Kitaev magnetism in layered halides. *Appl. Sci. Conver. Technol.* **30**, 191–194 (2021).
- [40] Zhang, Y., Lin, L.-F., Moreo, A. & Dagotto, E. Theoretical study of the crystal and electronic properties of  $\alpha$ -RuI<sub>3</sub>. *Phys. Rev. B* **105**, 085107 (2022).
- [41] Park, S.-Y. *et al.* Emergence of the isotropic Kitaev honeycomb lattice with two-dimensional Ising universality in  $\alpha$ -RuCl<sub>3</sub>. *Preprint at <https://arxiv.org/abs/1609.05690>* (2016).
- [42] Eichstaedt, C. *et al.* Deriving models for the Kitaev spin-liquid candidate material  $\alpha$ -RuCl<sub>3</sub> from first principles. *Phys. Rev. B* **100**, 075110 (2019).
- [43] Sandilands, L. J. *et al.* Spin-orbit excitations and electronic structure of the putative Kitaev magnet  $\alpha$ -RuCl<sub>3</sub>. *Phys. Rev. B* **93**, 075144 (2016).
- [44] Bachus, S. *et al.* Thermodynamic perspective on field-induced behavior of  $\alpha$ -RuCl<sub>3</sub>. *Phys. Rev. Lett.* **125**, 097203 (2020).
- [45] Riedl, K., Li, Y., Valentí, R. & Winter, S. M. Ab initio approaches for low-energy spin Hamiltonians. *Phys. Status Solidi B* **256**, 1800684 (2019).
- [46] Stavropoulos, P. P., Liu, X. & Kee, H.-Y. Magnetic anisotropy in spin-3/2 with heavy ligand in honeycomb Mott insulators: Application to CrI<sub>3</sub>. *Phys. Rev. Research* **3**, 013216 (2021).

- [47] Rousochatzakis, I., Reuther, J., Thomale, R., Rachel, S. & Perkins, N. B. Phase diagram and quantum order by disorder in the Kitaev  $K_1$ - $K_2$  honeycomb magnet. *Phys. Rev. X* **5**, 041035 (2015).
- [48] Rusnačko, J., Gotfryd, D. & Chaloupka, J. Kitaev-like honeycomb magnets: Global phase behavior and emergent effective models. *Phys. Rev. B* **99**, 064425 (2019).
- [49] Chaloupka, J. & Khaliullin, G. Magnetic anisotropy in the Kitaev model systems  $\text{Na}_2\text{IrO}_3$  and  $\text{RuCl}_3$ . *Phys. Rev. B* **94**, 064435 (2016).
- [50] Blöchl, P. E. Projector augmented-wave method. *Phys. Rev. B* **50**, 17953–17979 (1994).
- [51] Kresse, G. & Joubert, D. From ultrasoft pseudopotentials to the projector augmented-wave method. *Phys. Rev. B* **59**, 1758–1775 (1999).
- [52] Kresse, G. & Hafner, J. Ab initio molecular dynamics for liquid metals. *Phys. Rev. B* **47**, 558–561 (1993).
- [53] Kresse, G. & Furthmüller, J. Efficiency of ab-initio total energy calculations for metals and semiconductors using a plane-wave basis set. *Comput. Mater. Sci.* **6**, 15–50 (1996).
- [54] Blaha, P., Schwarz, K., Madsen, G. K. H., Kvasnicka, D. & Luitz, J. *WIEN2k, an augmented plane wave plus local orbitals program for calculating crystal properties (Techn. Universität Wien, Austria)* (2001).
- [55] Perdew, J. P., Burke, K. & Ernzerhof, M. Generalized gradient approximation made simple. *Phys. Rev. Lett.* **77**, 3865–3868 (1996).
- [56] Anisimov, V. I., Solov'ev, I. V., Korotin, M. A., Czyżyk, M. T. & Sawatzky, G. A. Density-functional theory and  $\text{NiO}$  photoemission spectra. *Phys. Rev. B* **48**, 16929–16934 (1993).
- [57] Aryasetiawan, F. *et al.* Frequency-dependent local interactions and low-energy effective models from electronic structure calculations. *Phys. Rev. B* **70**, 195104 (2004).
- [58] Aryasetiawan, F., Karlsson, K., Jepsen, O. & Schönberger, U. Calculations of Hubbard  $U$  from first-principles. *Phys. Rev. B* **74**, 125106 (2006).
- [59] Jiang, H. *et al.* FHI-gap: A GW code based on the all-electron augmented plane wave method. *Computer Phys. Commun.* **184**, 348–366 (2013).
- [60] Eschrig, H. & Koepnick, K. Tight-binding models for the iron-based superconductors. *Phys. Rev. B* **80**, 104503 (2009).
- [61] Koepnick, K. & Eschrig, H. Full-potential nonorthogonal local-orbital minimum-basis band-structure scheme. *Phys. Rev. B* **59**, 1743–1757 (1999).
- [62] Neese, F. The ORCA program system. *Wiley Interdiscip. Rev. Comput. Mol. Sci.* **2**, 73–78 (2012).
- [63] Neese, F. Efficient and accurate approximations to the molecular spin-orbit coupling operator and their use in molecular g-tensor calculations. *J. Chem. Phys.* **122**, 034107 (2005).
- [64] Mazin, I. I., Jeschke, H. O., Foyevtsova, K., Valentí, R. & Khomskii, D. I.  $\text{Na}_2\text{IrO}_3$  as a molecular orbital crystal. *Phys. Rev. Lett.* **109**, 197201 (2012).
- [65] Foyevtsova, K., Jeschke, H. O., Mazin, I. I., Khomskii, D. I. & Valentí, R. Ab initio analysis of the tight-binding parameters and magnetic interactions in  $\text{Na}_2\text{IrO}_3$ . *Phys. Rev. B* **88**, 035107 (2013).
- [66] Mu, S. *et al.* Role of the third dimension in searching for Majorana fermions in  $\alpha$ - $\text{RuCl}_3$  via phonons. *Phys. Rev. Research* **4**, 013067 (2022).